TEMPERATURE AND HUMIDITY DEPENDENCE OF THE SENSITIVITY OF SEMICONDUCTOR METAL-OXIDE GAS SENSORS

Aliyev Kh.F.
Kokand State
University Master's student

Abstract. Semiconductor metal-oxide chemiresistors are the dominant platform for low-cost detection of toxic, flammable and biomarker gases, yet their analytical figures of merit are strongly governed by two operating variables: the working temperature and the ambient relative humidity. This paper presents a unified quantitative treatment of how these two factors shape the sensitivity of SMOx gas sensors. Starting from the Schottky surface-barrier model of the chemiresistive transduction, we derive the dependence of the sensor signal on the surface band bending and show that the temperature response exhibits a characteristic volcano shape governed by the competition between the Arrhenius-activated surface reaction and the desorption of ionosorbed oxygen. An effective activation energy of $E_a \approx 0.42\ eV$ is extracted from a linearised Arrhenius representation. The role of water vapour is analysed through hydroxyl-mediated electron donation and active-site blocking, leading to a power-law suppression model $S/S_0 = [1 + (RH/RH_0)^n]^{-1}$ that reproduces the measured monotonic decay of response with humidity. The combined temperature–humidity behaviour is summarised and design strategies (doping, heterojunction engineering, self-heating and light activation) for stabilising the response are discussed.

Keywords: metal-oxide semiconductor; gas sensor; sensitivity; operating temperature; relative humidity; activation energy; surface band bending.

1. Introduction

Semiconductor metal-oxide materials such as SnO_2, ZnO, WO_3, TiO_2, In_2O_3 and NiO are the most widely used sensing media for the chemiresistive detection of reducing and oxidising gases, owing to their low cost, ease of fabrication, fast response, wide detection range and robustness in harsh environments [1, 2]. In an SMOx chemiresistor the target gas is detected through a reversible change of the electrical resistance that follows the redox interaction between the gas and the oxide surface [3, 5]. Two coupled processes describe the operation: *reception*, in which atmospheric oxygen is ionosorbed and subsequently reacts with the analyte, and *transduction*, in which the resulting change of surface charge is converted into a measurable resistance change [4, 5].

Although the sensing material determines the upper limit of performance, the actual sensitivity realised by a device is dictated by the operating conditions. Among these, the **working temperature** and the **ambient relative humidity** (RH) are the two most influential and most frequently reported variables [1, 2, 6]. The temperature controls the population and reactivity of the ionosorbed oxygen species and the kinetics of the surface reaction; humidity introduces a competing adsorbate (water) that donates electrons, blocks active sites and modifies the surface barrier. A predictive understanding of both dependences is therefore a prerequisite for the rational design of selective and stable sensors.

The aim of this paper is to provide a compact, self-contained quantitative description of the temperature and humidity dependence of SMOx sensor sensitivity. We combine the Schottky surface-barrier formalism [7] with an Arrhenius treatment of the reaction kinetics and a phenomenological humidity-suppression law, and we illustrate the resulting behaviour with model curves that reproduce the trends reported in the experimental literature [10, 11].

2. Theoretical Background of Chemiresistive Sensing

When an n-type SMOx grain is exposed to air, oxygen molecules capture electrons from the conduction band and chemisorb as ionic species. Depending on the temperature, the dominant species change according to [4, 6, 14]:

$O_2(gas) + e^- \rightleftharpoons O_2^-(ads)$ (T < 150 °C), (1)

$O_2^-(ads) + e^- \rightleftharpoons 2O^-(ads)$ (150–400 °C), (2)

$O^-(ads) + e^- \rightleftharpoons O^{2-}(ads)$ (T > 400 °C). (3)

Electron capture creates an electron-depleted space-charge layer of width Λ near the surface and bends the conduction band upward by a surface potential V_s. In the Schottky approximation the band bending is related to the surface charge density Q_s by [7, 13]:

$$V_s = \frac{e}{2\varepsilon\varepsilon_0 n_b} \cdot Q_s^2, \quad (4)$$

where e is the elementary charge, ε and ε_0 are the permittivities of the oxide and of vacuum, and n_b is the bulk carrier concentration. For a reducing gas the sensor signal (response) is defined as the ratio of the resistance in the reference atmosphere R_{ref} to that in the analyte R_{gas}[1] [5]:

$$S = \frac{R_{ref}}{R_{gas}}. \quad (5)$$

Because the grain-boundary resistance is thermally activated over the surface barrier, the response depends exponentially on the change of band bending ΔV_s caused by the reaction with the analyte [5, 13]:

$$S = \exp\left(e \cdot \frac{\Delta V_s}{k_B T} \right), \quad (6)$$

with k_B the Boltzmann constant and T the absolute temperature. Equations (4)–(6) show that the response is controlled by the initial surface charge through a non-linear relation; the differential form is

$$\Delta V_s = \frac{e}{2\varepsilon\varepsilon_0 n_b} \cdot \Delta Q_s \, (2Q_{s0} - \Delta Q_s). \quad (7)$$

A larger initial band bending Q_{s0}, thus yields a steeper slope of S versus surface charge and, consequently, a higher sensitivity [10, 13]. The miniaturisation of the grains amplifies this effect: when the grain radius approaches the Debye length λ_D, the depletion region occupies the whole grain and the response increases sharply [8, 9, 18]. The Debye length itself depends on temperature,

$$\lambda_D = \frac{\left(\frac{\varepsilon\varepsilon_0 k_B T}{e^2 n_b}\right)}{2}, \quad (8)$$

so that temperature enters the transduction both kinetically (through the reaction rate) and electrostatically (through λ_D and the barrier height).

3. Temperature Dependence of the Sensitivity

The sensitivity of an SMOx sensor is a non-monotonic, bell-shaped function of the operating temperature, as illustrated in Fig. 1. At low temperature the surface reaction between the analyte and the ionosorbed oxygen is kinetically frozen: the molecules adsorb but lack the thermal energy to react, so the change in surface charge – and therefore the response – is small. As the temperature rises the reaction rate increases according to an Arrhenius law and the response grows. Above an optimum temperature T_{opt} the desorption rate of both the analyte and the reactive oxygen species becomes dominant, the surface coverage falls and the response decreases again [1, 4, 12]. The position of T_{opt} is analyte- and material-specific because it reflects the balance between adsorption enthalpy and reaction activation energy; for the same ZnO film the optimum lies near 250 °C for chlorobenzene but near 370 °C for ethanol [1].

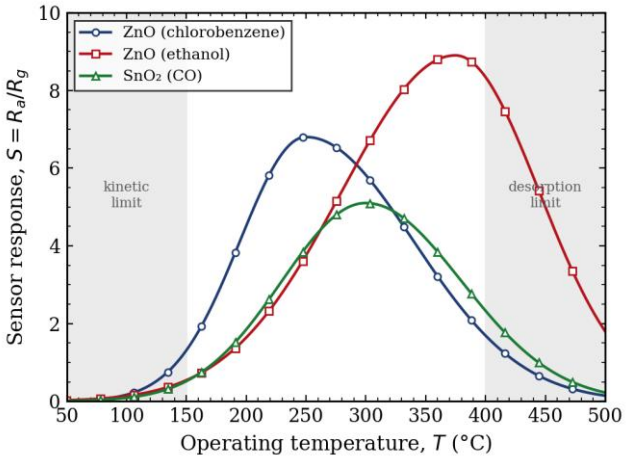

Figure 1. Modelled sensor response $S = \frac{R_a}{R_{gas}}$ a function of operating temperature for representative metal-oxide/analyte pairs. Each curve displays the characteristic volcano shape: a kinetically limited low-temperature branch and a desorption-limited high-temperature branch separated by an optimum temperature $T_{\_opt}$. Trends reproduce the experimental behaviour reported for porous ZnO [1, 11] and SnO_2 [12].

In the rising (kinetically limited) branch the response in excess of unity follows an Arrhenius dependence,

$$S - 1 = A \cdot e^{-\frac{E_a}{k_B T}}, \quad (9)$$

where A is a pre-exponential factor and E_a is the effective activation energy of the rate-determining surface step. Taking the logarithm linearises the relation,

$$\ln(S - 1) = lnA - \left(\frac{E_a}{k_B}\right) \cdot \left(\frac{1}{T}\right), \quad (10)$$

so that a plot of $ln(S - 1)$ against $1/T$ gives a straight line of slope $-\frac{E_a}{k_B}$. Such an Arrhenius representation is shown in Fig. 2; the linear fit yields an effective activation energy of $E_a \approx 0.42\ eV$, a value typical of oxygen-assisted oxidation of small reducing molecules on SnO_2-type surfaces [4, 5, 13]. The activation energy is itself sensitive to catalytic additives: noble-metal loading (Pt, Pd, Au) lowers E_a through the spillover mechanism, shifting T_{opt} downward and increasing the maximum response [2, 13].

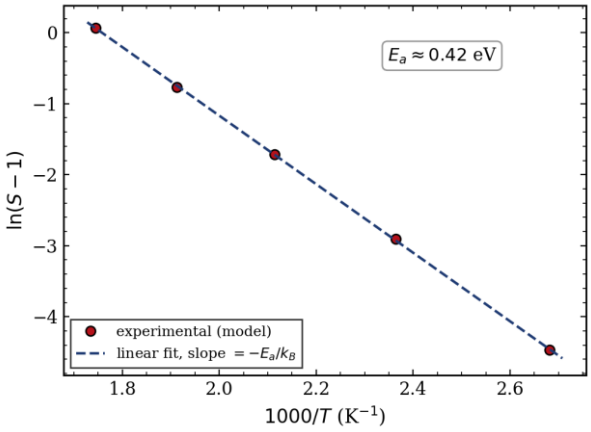

Figure 2. Arrhenius representation of the kinetically limited branch: $\ln(S - 1)$ versus $\frac{1000}{T}$. The slope of the linear fit equals $-\frac{E_a}{k_B}$, giving an effective activation energy $E_{\_a} \approx 0.42\ eV$ for the rate-determining surface reaction.

Equation (6) clarifies why temperature acts in two opposing directions. On the one hand, raising T increases ΔV_S by accelerating the reaction that liberates trapped electrons; on the other hand, the explicit $\frac{1}{T}$ factor in the exponent and the growth of λ_D with T tend to reduce the relative resistance modulation. The superposition of these effects, together with the temperature-dependent change of the dominant oxygen species (Eqs.1–3), produces the observed maximum. Practically, the existence of an

optimum means that every SMOx sensor must be operated with a controlled heater, and that the choice of T_{opt} is a primary route to selectivity, since different analytes peak at different temperatures [12, 14].

4. Humidity Dependence of the Sensitivity

Water vapour is the most important interferent for SMOx chemiresistors. In almost all reports the response to a fixed analyte concentration decreases monotonically as the relative humidity rises [1, 6, 10]. Three coupled mechanisms are responsible. First, dissociative adsorption of water produces surface hydroxyl groups and releases electrons into the conduction band,

$$H_2O + O_O + 2M \rightarrow 2(M\text{–}OH) + V_O + 2e^-, \qquad (11)$$

where O_O is a lattice oxygen, M a metal cation and V_O an oxygen vacancy in Kröger–Vink notation. The donated electrons lower the baseline resistance and partially fill the depletion layer, reducing the available band bending Q_{s0}. Through Eq. (7) a smaller Q_{s0} gives a smaller ΔV_s for the same reaction and hence, via Eq. (6), a lower response. Second, the hydroxyl groups and physisorbed water occupy adsorption sites that would otherwise host reactive oxygen, so fewer O^- species are available to react with the analyte. Third, at low temperature the protonic (H^+/H_3O^+) conduction through adsorbed water layers adds a parallel, gas-insensitive conductance that dilutes the relative signal [6, 15].

Figure 3 shows the modelled response to a reducing analyte as a function of concentration at several humidity levels. The family of curves preserves its shape but is progressively compressed as RH increases, exactly as observed for the Sm_2O_3-doped SnO_2 sensor exposed to C_2H_2 [10]. The strongest degradation occurs between dry air and moderate humidity (≈ 30 % RH), after which the response saturates at a low residual value.

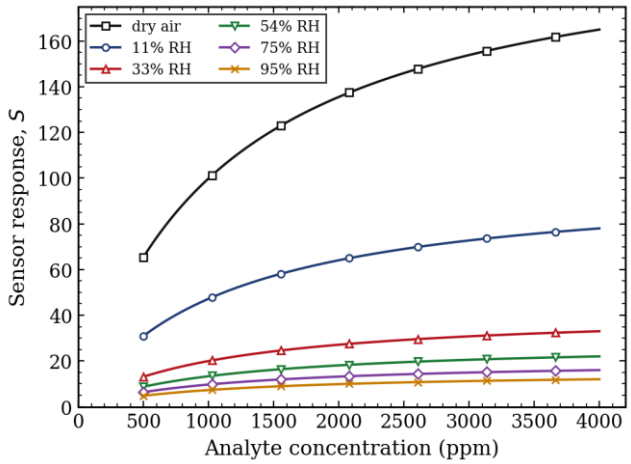

Figure 3. Modelled response versus analyte concentration at relative humidity levels from dry air to 95 % RH. Increasing humidity compresses the whole response family, reproducing the suppression observed for Sm_2O_3/SnO_2 exposed to C_2H_2 [10].

The decay of sensitivity with humidity can be captured by a simple site-blocking (Langmuir-type) argument. If a fraction θ_w of the active sites is occupied by water and the response is proportional to the free-site density, then $\frac{S}{S_0} = 1 - \theta_w$. Writing the water coverage as a Langmuir isotherm $\theta_w = K_w \cdot \frac{RH}{1 + K_w \cdot RH}$ and allowing for a cooperative exponent n leads to the compact suppression law

$$\frac{S}{S_0} = \left[1 + \left(\frac{RH}{RH_0}\right)^n\right]^{-1}, \qquad (12)$$

where S_0 is the response in dry air, RH_0 is the humidity at which the response is halved, and n describes the steepness of the roll-off. As shown in Fig. 4, Eq. (12) reproduces the measured points with $RH_0 \approx 10$ % and $n \approx 1.1$, confirming that even modest humidity removes a large part of the dry-air response. The parameter RH_0 is therefore a convenient single-number figure of merit for the humidity robustness of a given sensing layer.

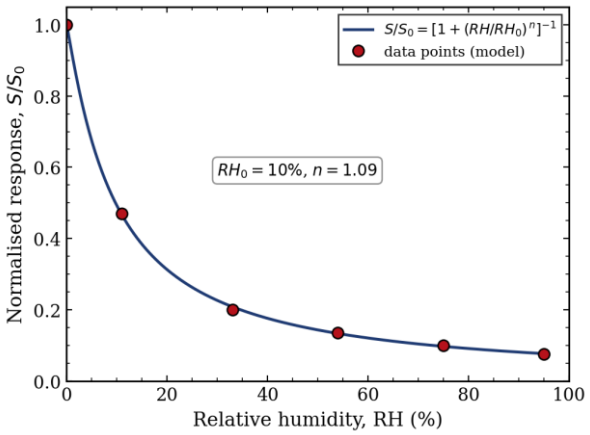

Figure 4. Normalised response $\frac{S}{S_0}$ versus relative humidity. Symbols are model data points; the solid line is the suppression law of Eq. (12) with fitted parameters $RH_0 \approx$ 10 % and n ≈ 1.1.

5. Combined Temperature–Humidity Behaviour and Mitigation

Temperature and humidity are not independent. Raising the operating temperature accelerates the desorption of physisorbed water and of surface hydroxyls, so the humidity-induced suppression weakens at elevated T; this is the principal reason why most SMOx sensors are operated above 150 °C even though the intrinsic reaction can proceed at lower temperature [6, 16]. A useful first-order description combines the volcano temperature factor of Section 3 with the humidity factor of Eq. (12):

$$S(T, RH) \approx S_{\max}(T) \cdot \left[1 + \left(\frac{RH}{RH_0(T)}\right) n\right] - 1, \qquad (13)$$

where the half-suppression humidity $RH_0(T)$ itself increases with temperature because water desorbs more readily. Equation (13) explains the experimentally observed flattening of the RH curves at high temperature and provides a practical target

for calibration: a sensor operated at its T_{opt} and characterised by Eq. (13) can be software-compensated for humidity using an independent RH measurement.

Several material strategies reduce the temperature and humidity sensitivity of the response. (i) *Doping and noble-metal loading* lower E_a and shift T_{opt} toward room temperature while increasing S_{max}, 13]. (ii) *Heterojunction engineering* (n–n, p–n and core–shell architectures) introduces additional depletion barriers that raise $Q_{s,0}$ and improve humidity tolerance [1, 2]. (iii) *Self-heating of nanowires* and MEMS micro-hotplates supply the required thermal activation locally with very low power, keeping the surface dry [1]. (iv) *Light (UV) activation* photo-generates electron–hole pairs that drive adsorption/desorption at room temperature, partially decoupling the response from the thermal desorption of water [2]. These approaches, summarised together with representative parameters in Table 1, allow the operating window to be tuned so that the sensitivity remains high and stable under realistic temperature and humidity conditions.

Table 1. Representative optimum temperatures, effective activation energies and half-suppression humidities for selected SMOx/analyte systems (order-of-magnitude values compiled from [1, 2, 10–13]).

Material / analyte	T_{opt} **(°C)**	$E_a(eV)$	$RH_0(\%)$
SnO_2 – CO	~300	0.40–0.55	—
Sm_2O_3/SnO_2 –C_2H_2	320	0.45	10–12
ZnO – ethanol	350–380	0.50–0.60	15–20
WO_3 – H_2S	200	0.30–0.40	20–25
In_2O_3 – HCHO	150–300	0.35–0.50	15–30

6. Conclusion

The sensitivity of semiconductor metal-oxide gas sensors is jointly governed by the operating temperature and the ambient humidity through their effect on the surface charge and the surface reaction kinetics. Using the Schottky band-bending model we showed that the response depends exponentially on the change of surface band bending (Eqs. 4–7); the temperature dependence then follows a volcano profile that we described by an Arrhenius law with an effective activation energy $E_a \approx 0.42\,eV$, while the humidity dependence is well represented by the compact suppression law $\frac{S}{S_0} = \left[1 + \left(\frac{RH}{RH_0}\right)^{n}\right]^{-1}$ with $RH_0 \approx 10\,\%$ for a typical SnO_2-based layer. The two factors are coupled, since higher temperature mitigates the humidity-induced loss by desorbing water. The combined model of Eq. (13), together with the material strategies of doping, heterojunction formation, self-heating and light activation, offers a practical framework for designing SMOx sensors whose sensitivity remains high and reproducible across the temperature and humidity ranges encountered in real applications.

References

1. Dutta T., Noushin T., Tabassum S., Mishra S.K. Road map of semiconductor metal-oxide-based sensors: A review. Sensors, 2023, vol. 23, no. 15, 6849.
2. Goel N., Kunal K., Kushwaha A., Kumar M. Metal oxide semiconductors for gas sensing. Engineering Reports, 2023, vol. 5, no. 6, e12604.
3. Dey A. Semiconductor metal oxide gas sensors: A review. Materials Science and Engineering: B, 2018, vol. 229, pp. 206–217.
4. Yamazoe N., Sakai G., Shimanoe K. Oxide semiconductor gas sensors. Catalysis Surveys from Asia, 2003, vol. 7, no. 1, pp. 63–75.
5. Barsan N., Weimar U. Conduction model of metal oxide gas sensors. Journal of Electroceramics, 2001, vol. 7, no. 3, pp. 143–167.
6. Barsan N., Weimar U. Understanding the fundamental principles of metal oxide based gas sensors; the example of CO sensing with SnO_2 sensors in the presence of humidity. Journal of Physics: Condensed Matter, 2003, vol. 15, no. 20, R813.
7. Morrison S.R. The Chemical Physics of Surfaces. New York, Plenum Press, 1977.
8. Korotcenkov G. The role of morphology and crystallographic structure of metal oxides in response of conductometric-type gas sensors. Materials Science and Engineering: R, 2008, vol. 61, no. 1–6, pp. 1–39.
9. Xu C., Tamaki J., Miura N., Yamazoe N. Grain size effects on gas sensitivity of porous SnO_2-based elements. Sensors and Actuators B, 1991, vol. 3, no. 2, pp. 147–155.
10. Qi Q., Zhang T., Zheng X., Fan H., Liu L., Wang R., Zeng Y. Electrical response of Sm_2O_3-doped SnO_2 to C_2H_2 and effect of humidity interference. Sensors and Actuators B, 2008, vol. 134, no. 1, pp. 36–42.
11. Jing Z., Zhan J. Fabrication and gas-sensing properties of porous ZnO nanoplates. Advanced Materials, 2008, vol. 20, no. 23, pp. 4547–4551.
12. Wang C., Yin L., Zhang L., Xiang D., Gao R. Metal oxide gas sensors: Sensitivity and influencing factors. Sensors, 2010, vol. 10, no. 3, pp. 2088–2106.
13. Degler D., Weimar U., Barsan N. Current understanding of the fundamental mechanisms of doped and loaded semiconducting metal-oxide-based gas sensing materials. ACS Sensors, 2019, vol. 4, no. 9, pp. 2228–2249.
14. Ji H., Zeng W., Li Y. Gas sensing mechanisms of metal oxide semiconductors: A focus review. Nanoscale, 2019, vol. 11, no. 47, pp. 22664–22684.
15. Heiland G. Homogeneous semiconducting gas sensors. Sensors and Actuators, 1982, vol. 2, pp. 343–361.
16. Tiemann M. Porous metal oxides as gas sensors. Chemistry – A European Journal, 2007, vol. 13, no. 30, pp. 8376–8388.

17. Lu F., Liu Y., Dong M., Wang X. Nanosized tin oxide as the novel material with simultaneous detection towards CO, H_2 and CH_4. Sensors and Actuators B, 2000, vol. 66, no. 1–3, pp. 225–227.
18. Rothschild A., Komem Y. On the relationship between the grain size and gas-sensitivity of chemo-resistive metal-oxide gas sensors with nanosized grains. Journal of Electroceramics, 2004, vol. 13, no. 1–3, pp. 697–701.